Contents lists available at ScienceDirect

Chemical Engineering Research and Design

journal homepage: www.elsevier.com/locate/cherd

Analysis of the performance of concentrated solar power facilities using different thermal fluids

*Sebastián García, Mariano Martín**

Departamento de Ingeniería Química, Universidad de Salamanca, Pza. Caídos 1-5, 37008 Salamanca, Spain

ARTICLE INFO

Article history:
Received 27 July 2020
Received in revised form 14 January 2021
Accepted 26 January 2021
Available online 8 February 2021

Keywords:
Solar energy
Concentrated solar power
Thermal fluids
Rankine cycle
Mathematical Optimization

ABSTRACT

A systematic comparison of the performance and economics of concentrated solar power plants using various heat transfer fluids including molten salts and synthetic fluids (Dowtherm A, Syltherm, HELISOL, Malotherm and Therminol VP1) is carried out. First, a process systems approach is used to determine the yield of the thermodynamic cycle using different thermal fluids, their operating conditions and the water consumption. Next, an economic evaluation is performed. For reference Almería, to the South of Spain, is the location selected because of the high solar irradiance. The efficiency of the regenerative Rankine cycle increases with the maximum operating temperature. The average power production increases from 16 MW using Malotherm to 25 MW using the molten salts, while the water consumption decreases from 3.6 L/kWh to 2.1 L/kWh. A higher efficiency results in more competitive electricity prices that decrease from 0.21 €/kWh (Malotherm) to 0.12 €/kWh (molten salts) with the maximum operating temperature. Furthermore, the effect of the maximum temperature on power and water consumption are computed towards a pre-evaluation of novel fluids under development.

1. Introduction

Solar energy is the most abundant resource on Earth. However, the low intensity and scattered availability results in the need to transform it into a handy form of energy, electricity (Martín and Martín, 2013; Martin, 2015). Two main technologies are widely used, photovoltaic panels (PV solar) and concentrated solar power facilities (CSP). The first one has gained attention due to the subsidies to install PV panels as well as their simple operation. However, they can only produce electricity during daytime. CSP plants offer the possibility of operating overnight by means of storage systems. The hourly and daily variation in solar availability are buffered using thermal storage systems. Typically, a heat transfer fluid (HTF) is heated up using solar energy and stored during the sun hours for its use overnight (International Energy Agency (IEA), 2010). For longer term operation, hybrid systems combining a backup source, such as a natural gas boiler or recently biomass (Vidal and Martín, 2015) and waste (de la Fuente and Martín, 2019), with the CSP facility are used. In this work we focus on thermal storage systems for overnight operation.

Concentrated solar power facilities typically consist of the solar field, the energy storage system, the power island, and the cooling system. A number of studies have covered each one individually and / or the analysis of the entire facility. Reviews on the configuration and design of solar fields can be found in the literature (International Energy Agency (IEA), 2010; NREL 2011). Parabolic troughs and solar towers are the most extended designs (NREL 2011; Zhang et al., 2013). The optimal lay-out of the heliostats has been addressed by different groups using mathematical or algorithmic approaches (Mutuberria et al., 2015; Noone, et al., 2012; Barberena et al., 2016; Leonardi et al., 2019; Collado and Guallar, 2019; Schell 2011). The analysis of the thermodynamic cycle has focused most of the research. Simulation (Janjai et al., 2011; Halb et al., 2012; Li et al., 2019) or optimization approaches have been used for the evaluation of the performance of the cycle. Within the optimization one, model-based optimization (Morin et al., 2010; Montes et al., 2009a, b; Mahmoudimehr and Sebhati 2019; Yagli et al., 2019), neural networks (Richter et al., 2011) and mathematical optimization (Martin, 2015; Ghobeity et al., 2011; Slocum et al., 2011) have been used. Cooling is a critical part of these systems since CSP facilities are meant to be installed in places with low availability of water. Cooling towers (Martin and Martín, 2017; Halb et al., 2012; Martin and Martín, 2017) and dry systems such as A-frames (Luceño and Martín, 2018) or dry cooling towers (Tanimizu and Hooman, 2013) have been studied and compared (Palenzuela et al., 2013) to evaluate the water and power consumption

* *Corresponding author.*
E-mail address: mariano.m3@usal.es (M. Martín).
https://doi.org/10.1016/j.cherd.2021.01.030

Nomenclature

A	Specific area (m^{-1})
A_{field}	Area of the heliostat field (m^2)
A_h	Area of a heliostat (120 m^2)
$area_{sup}$	Superficial area provided by the heliostat field (m^2)
$Area_{helio}$	Area of a heliostat (m^2)
b	Aggregation state (liquid, steam)
B	Water blowdown flow (kg/s)
COC	Cycles of concentration concentration
c_p	Heat capacity (kJ/kg/K)
c_h	Humid air heat capacity (kcal/kg $_{dry\ air}$)
E_s	Energy received from the Sun (kJ)
Ev	evaporation flow (kg/s)
$fc_{(J,unit,unit1)}$	Mass flow of component J from unit to unit1 (kg/s)
$H_{b,(unit,unit1)}$	Enthalpy of the stream at the state b from the stream from unit to unit1 kJ/kg
$H_{steam(isoentropy)}$	Enthalpy of the stream at the if the expansion is isentropic kJ/kg
h_l	Resistance to heat transfer (kcal/m^2·s)
H	Humid air enthalpy (kcal/kg)
h_{sun}	Sun hours (h)
k_y	Resistance to mass transfer (kg /m^2s)
L/V	Ratio between the water and the air flow rates across the column in mass
Load	Fraction with respect to the design conditions
n_h	Number of heliostats
Nd_{ays}	Number of days of the particular month
N_{helios}	Number of heliostats
Operating	Operating hours in a year /6450/
Power	Mean power (MW)
p_{turbi}	Inlet pressure to body i in the turbine (bar)
P	Pressure (bar)
$P_{v,\ sat}$	Vapor pressure (mmHg)
$Q_{(collector)}$	Energy captured by collector (kW)
$Q_{(unit)}$	Energy at heat exchanger unit (kW)
E_s	Solar energy (J)
Rad_{annual}	Annual radiation (kW/m2)
radiation	Average annual radiation in the sun hours MWh per m2 and day
Rad_{annual}	Average annual radiation MWh/m2
$rend_{field}$	Field efficiency /0.55/
$rend_{helio}$	Heliostat efficiency (0.9)
$s_{b(unit,unit1)}$	Entropy the stream at the state b for the stream from unit to uni1 kJ/kgK
S	Cross sectional area (m2)
sun_{hour}	Hours of sun a day
t_d	days in a month (days)
t	Operating time (s) /8760 h)
T (unit1, unit2)	Temperature of the stream from unit 1 to unit 2 (°C)
t_L	Liquid temperature inside cooling tower(°C)
T	Air temperature across the cooling tower (°C)
$T_{turbimin}$	Saturating temperature at exit of body i (°C)
$T_{(unit,unit1)}$	Temperature of the stream from unit to unit 1 (°C)
tp	time period
Wa	Component Water
$W_{(unit)}$	Work generated or needed at unit (kW)
$Y_{i,sat}$	Saturated moisture (kg moisture per kg dry air)
Z	Height of the column (m)
z	Objective function (kW)

Symbols

η_{helios}	Efficiency of the heliostats
η_{filed}	Field efficiency
η_s	Isentropic efficiency
η_{real}	Operating efficiency of the turbine
υ	Loss of efficiency due to fractional load to the turbine

associated with the operation to determine the selection of the technology as a function of the availability of water (Martin and Martín, 2017). In spite of the low water availability, wet cooling towers are the most efficient technology in many regions (Luceño and Martín, 2018). However, there is still a particular challenge to be further evaluated, the performance of the HTF's.

Solar irradiance is absorbed by a fluid such as synthetic fluids, molten salts or water (International Energy Agency (IEA), 2010, NREL, 2011, Yagli et al., 2019) that is the first stage in the conversion of the energy harvested from the Sun to electricity. Even though the storage system presents several additional challenges, due to the energy losses (Sole et al., 2018), and the dynamics of the storage (Crespi et al., 2018), the yield of the facility relies on the performance of the thermal fluid. Direct and indirect storage systems are available, whether the heat transfer fluid is the same as that used for power production or not. Indirect storage is the most common technology based on its higher efficiency (NREL, 2011). Several reviews on storage systems compare qualitatively various media (sensible, latent and thermochemical) in terms of properties, maturity of the technology and stability (Kuravi et al., 2013). Among them, those based on sensible heat including synthetic fluids, water and salts are the ones used at commercial scale CSP facilities. Molten salts are widely used due to the high operating temperature. However, they present operating issues because the salts crystalize at 238 °C and solidify at 221 °C (NREL, 2011), and they are corrosive (Fernández et al., 2012). Alternatively, synthetic fluids, organics and silicones, can be used, but their operating temperatures are limited to 425 °C (Dowling et al., 2017). Over the last years several works have compared the use of different synthetic fluids (Jung et al., 2015), different salts (Polimeni et al., 2018) and different salt systems (Sau et al., 2016) from a thermodynamic perspective. Even though there has been a lot of modelling work on the performance of CSP plants, to the best of the authors' knowledge there is no systematic techno-economic analysis comparing the operation of entire plants using different heat transfer fluids with the same Rankine cycle. In addition, due to the particular allocation of CSP facilities in arid areas, the water consumption of the cycles operating with the different HTF's is also computed.

A process systems approach is used for the comparison of the performance of concentrated solar power plants using six thermal fluids, molten salts and five synthetic fluids, including silicones and organic fluids. The transfer fluids are analyzed in terms of the power produced, the water consumed per kWh and the facility investment and electricity production costs. The rest of the paper is organized as follows. Section 2 describes the flowsheet of the process and the modelling assumptions. In section 3 the solution procedure is presented. Next, in section 4 the main results of the operation of the various CSP plants are presented, including pressures, temperatures as well as the water consumption of the facility for the different thermal fluids. Subsequently, the estimation of the investment and electricity production costs are reported. Finally, section 5 draws the conclusions.

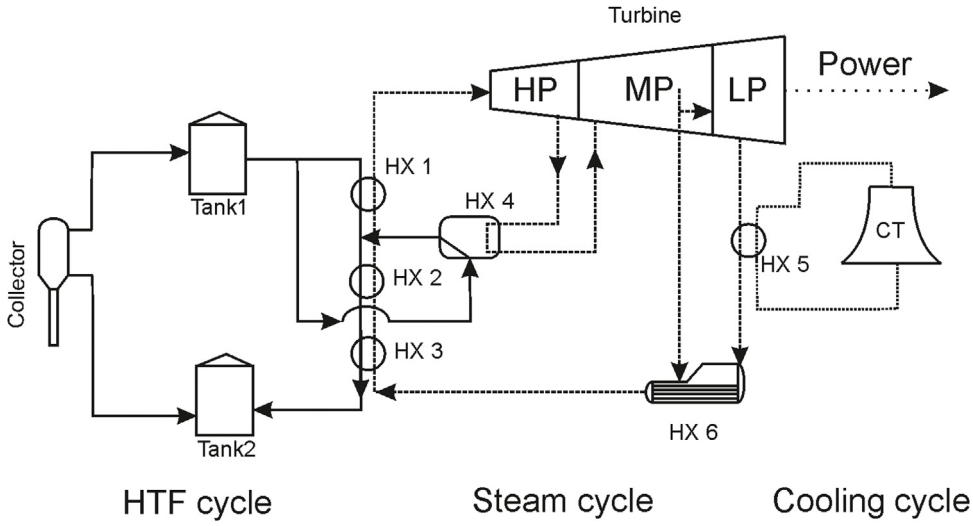

Fig. 1 – Flowsheet of the system. HP: High Pressure; MP: Medium pressure; LP: Low pressure. (-) HTF;(–) Steam; (··) Cooling water.

2. Process analysis

2.1. *Modeling assumptions*

The concentrated solar facility is divided into three sections. The heliostat field is not further analysed in this work but for its efficiency. The heat transfer fluids (HTF's) are heated-up at the collector and stored in tanks (Tank1&2) overnight for the operation of the plant. The HTF is used to generate steam for the Rankine cycle. Finally, a cooling system is considered. The cooling load and the water consumed are evaluated. Fig. 1 shows a process diagram of the facility for a regenerative Rankine cycle with reheating, based on typical CSP facilities and previous work (Martín and Martín, 2013). The production of steam is divided into three stages, compressed water heating (HX3), evaporation (HX2) and overheating (HX1). The steam fed to the high-pressure turbine (HP) is produced using only a fraction of the flow of HTF at high temperature from the storage tank. The rest of the flow of HTF is used to reheat up the expanded steam (HX4) before reinjecting it to the turbine at medium pressure (MP). Both streams of HTF are mixed and used for the evaporation (HX2) and compressed water heating (HX3). An extraction from the MP turbine is used to represent the extractions of the steam turbine. The extraction is used in the regeneration part of the cycle, reheating up the water. The rest of the steam is expanded in the low pressure (LP) turbine. The exhaust steam is condensed (HX5) and recycled. A natural draft cooling tower is used as a cooling technology based on its high efficiency (Luceño and Martín, 2018).

Each unit in the flowsheet is modeled using first principles, including mass and energy balances, thermodynamics of the fluids, steam and HTF's, and industrial rules of thumb (Martín, 2016). In this section we provide the modelling principles. For further details of the model of the process see the Appendix.

The solar field is modeled by the yield from solar incidence to thermal energy (Martin and Martín, 2017). Furthermore, apart from the operating temperature, the various thermal fluids show different heat capacities that characterize the heat transfer from the Sun to the HTF and from it to the generation of steam, affecting the flows across the units, and different film coefficients, determining the heat exchanger areas. Since a detailed mechanical design of the heat exchangers is not carried out, rules of thumb (Wallas, 1990) and the manufacturer's datasheets of the different fluids are used to estimate the film coefficients (Eastman, 2019; Dow, 2019a,b, Sasol, 2019). Two silicones, HELISOL and Syltherm, three synthetic organic fluids, Dowtherm A, Therminol VP1, Malotherm, and molten salts are used in the comparison.

The thermodynamics of the steam and the isentropic efficiency are used to compute the power obtained after each expansion. The efficiency of the turbine considers partial load operation by modelling the isentropic expansion efficiency using or developing empirical correlations from the literature (Jüdes et al., 2009) among the ones available in the literature (Jüdes et al., 2009; NREL, 2019; Erhart et al., 2011).

The cooling tower is modelled considering the mass transfer using the Mickley method to compute the water consumption of the process. The mechanical design of the tower is out of the scope of this work (Martin and Martín, 2017; Guerras and Martín, 2020).

2.2. *Weather conditions*

The operation of the facility relies on the weather conditions of the location. Table 1 shows the main features of the yearly climate of Almería, incldluing the irradiance, the sun hours, as well as the air temperature and moisture and the temperature of the water of the Mediterranean sea (JA, 2013). These conditions are selected to present a representative case study, but the model can be used to evaluate the performance of CSP plants in any other location using data from other sources or else, if not available, computed using predictive models (Ustun et al., 2020)

3. Solution procedure

The operating conditions at the units, the flows and the power production are computed by optimizing the model of the facility described in section 2 for different thermal fluids. The objective function is given in eq. (1) as the maximization of the power generated over the year using a monthly discretization, tp:

$$z = \sum_{tp} W_{(Turbine1,tp)} + W_{(Turbine2,tp)} + W_{(Turbine3,tp)} \quad (1)$$

Table 1 – Plant operating conditions (Anon, 2021a).

MONTH	kWh/m^2·day	Day	SUN (H)	Sun(h/day)	T Amb (^{o}C)	% Humidity	Twater (^{o}C)
Jau	4.377	31	191	6.161	12.5	69	15.5
Feb	5.125	28	191	6.821	13.2	68	15.0
Mar	5.319	31	228	7.355	14.7	66	16.0
Apr	6.387	30	250	8.333	16.4	64	17.5
May	6.697	31	299	9.645	19.1	66	19.5
Jun	8.587	30	322	10.733	22.7	64	25.0
Jul	8.668	31	338	10.903	25.7	63	26.0
Aug	7.342	31	312	10.065	26.4	65	27.0
Sep	6.057	30	257	8.567	24.0	66	26.0
Oct	4.126	31	221	7.129	20.0	68	24.0
Nov	3.513	30	187	6.233	16.2	70	21.0
Dec	3.326	31	176	5.677	13.7	70	17.0
Average	5.794	30.4	248	8.13	18.7	66.6	20.8

Subject to the model for the process described in section 2 and presented in the Appendix.

The problem formulated is a non-linear programming (NLP) one consisting of 263 equations and 284 continuous variables per month and fluid. It is written in GAMS where the decision variables are the flow rate, the pressure and temperature of all the streams across the process. In addition, several variables such as the fraction of the flow of HTF used to overheat the steam, HX1, the one needed to reheat the steam, HX4, or the air temperature profile across the cooling tower are of particular interest. The problem is optimized on a monthly basis, using a multistart optimization scheme with CONOPT 3.0 as solver.

Next, an economic evaluation is performed. The factorial method is used to estimate the production cost of the electricity and the investment cost of the facility (Sinnot, 1999). Regarding the investment cost, it considers the cost of the units involved in Fig. 1, as well as their installation, the piping and instrumentation, the cost for the ground, the chemicals, and the administration. The cost of the equipment is updated from the correlations presented in (Almena and Martín, 2015) except for the heliostats, whose cost is assumed to be 120 €/m^2. The design point for the units corresponds to an irradiation of 900 W/m^2 and the atmospheric conditions of July. A solar field consisting of 3900 heliostats is considered for all facilities to evaluate the efficiency of the HTF. The installation of the equipment is estimated as 0.5 times their cost. To estimate the cost of the piping, the isolation, the instrumentation and the infrastructure for the utilities factors of 0.2, 0.15, 0.2 and 0.1 times the equipment costs are assumed, to be consistent with previous work for comparison (Martín and Martín, 2013). Land and edifications cost are estimated to be 8 M€. The thermal fluids are stored such that the facility operates during the night. Thus, a certain volume is to be purchased of the salts (0.665 €/kg) (Martín and Martín, 2013) and the synthetic fluids, DTA, VP-1 and Syltherm and HELISOL (0.45 €/kg), Marlotherm (1 €/kg) (Anon, 2021b). It is estimated that the fees correspond to 3% of the fix cost. The overheads and administrative costs add up to 10% of the direct costs, computed as the fix cost and the fees, and the plant layout represent 5% of the fix cost. The plant start-up cost is estimated as 15% of the investment.

Electricity production cost is computed following the procedure in (Sinnot, 1999). The various items involved in the production cost are estimated as follows: labour is computed as 0.5% of the investment, the equipment maintenance adds up to 2.5% of the fix costs, amortization is estimated to be linear with time in 20 years, taxes and overheads represent 1% of the investment each and administration is estimated as 5% of labour, equipment maintenance, amortization, taxes and overheads (Martín and Martín, 2013).

4. Results

This section presents the discussion of the effect of the HTF's on the efficiency of the thermal cycle and the operating conditions, the water consumption, and the economic evaluation of the facilities operating with the different HTF's.

4.1. *Major operating conditions of the CSP plants*

The main operating conditions of the CSP plants for each of the HTF's evaluated are presented in Table 2. Those with the same maximum temperature show the same operating pressures and temperatures at the Rankine cycle. In addition, the maximum pressure at the turbine is directly related to the maximum operating temperature of the HTF. The maximum pressure at the HP turbine goes from 20.4 bar for Malotherm, with a highest operating temperature of 350 °C, to 30–31.5 bar for HELISOL, DTA, Syltherm and Therminol VP1 and up to 125 bar for the molten salts. However, for the medium pressure and low pressure all the synthetic fluids show the same pressures, 2.1–2.5 bar, 1.1 bar and 0.08 bar while the salts show larger pressures across the turbine, typically with a 1:5 ratio, but for the exhaust pressure. The fraction of salts required to overheat the steam increases with the maximum operating temperature, see Table 2, from 12% when the highest temperature is 350 °C to 16% for 400 °C and up to 36%. In the case of molten salts, whose maximum operating temperature is 565 °C. It could be possible to predict the fraction of HTF used for reheating for a particular fluid based on the results in Table 3. However, the extraction of stream from the turbine to heat up the condensed water is around 8–10%.

The values reported in Table 2 are compared with results from the literature. Most of the works reporting operating conditions for the Rankine cycle of CSP plants focus on Therminol VP1 or molten salts as HTF's separately. Even though in most cases a Rankine cycle with reheating is used, the turbine structure is not the same in all cases using mostly high- and low-pressure turbines, and the regeneration and reheating stage are sometimes not considered which makes the comparison among literature results and with ours not straightforward. For comparison, Table 3 shows the values reported in the literature. Note that the results in the literature are obtained in simulation-based studies. It can be seen that the operating pressure at the turbine increases with the maximum operating temperature of the HTF's, as it is presented

Table 2 – Main operating conditions of the 6 fluids.

	T(HP) (°C)	P(HP) (bar)	P(MP) (bar)		P(Ext) (bar)	P(exha) (bar)	% HTF Reheating	% Extraction
Dowtherm A	400	31.5	2.1	1.1		0.08	16	8
Syltherm	400	31.5	2.1	1.1		0.08	16	8
Therminol: VP1	400	31.5	2.1	1.1		0.08	16	8
Malotherm	350	20.4	2.1	1.1		0.135	12	8
Helisol	425	29	2.5	1.1		0.08	17	10
Salts	565	125	11	6.5		0.19	36	8

Table 3 – Literature operating conditions (Halb et al., 2012; Morin et al., 2010, Ghobeity et al., 2011; Nezammahalleh et al., 2010; Xu et al., 2011; Palenzuela et al., 2011).

HTF	T(HP) (°C)	P(HP) (bar)	P(MP) (bar)	P(Ext) (bar)	P(exha) (bar)	Reference
VP1	371	104	17	-	0.18	Palenzuela et al. (2011)
VP1	371	104	17	-	0.31	Palenzuela et al. (2011)
VP1	371	104	17	-	0.18	Palenzuela et al. (2011)
VP1	371	104	17	(2/4/6/10/16)	0.18	Palenzuela et al. (2011)
Salts	540	40	-	-	0.05	Ghobeity et al. (2011)
VP1	392.9	98.7	18.6	-	0.08	Morin et al. (2010)
VP1	373	100	18	-	0.06-0.2	Halb et al. (2012)
Salts	552	126	-	31	0.1	Xu et al. (2011)
Salts	552	126	-	31	0.1	Xu et al. (2011)
Salts	552	240	48	30	0.1	Xu et al. (2011)
None	500	90	18	7/2.1/0.5	0.07	Nezammahalleh et al. (2010)

in this work. However, for Therminol VP1, operating pressures around 100 bar are reported in the literature, while the optimization suggests values around 31 bar. Note that Palenzuela et al. (2011) use a high-medium pressure turbine alone, while Morin et al. (2010) show a more detailed thermodynamic cycle with high, medium and low pressure turbines. However, in both cases the medium pressure is around 18 bar versus the 2.1 the optimization suggests. Morin's work shows values of 2.73 and 0.96 at two of the medium and low-pressure turbine sections, similar to the ones shown in the optimization results. Halb et al. (2012) results are similar to the ones reported by Morin et al. (2010) using a high, medium and low-pressure turbine. With regards to the extractions, Halb et al. (2012) reported 24% while Morin et al. (2010) 19% vs the 8% that our results show. However, they considered a detailed simulation of the cycle versus the optimization we presented. In addition, Palenzuela et al. do not consider regeneration in the analysis of the cycle. In case of using molten salts, the optimization results report pressures similar to the values presented by Xu et al. (2011), a system that considers no reheating or regeneration and simulates the turbine as consisting of high- and low-pressure turbines, around 130 bar, but larger than the ones in Ghobeity et al. (2011) that shows 40 bar using a simplified regenerative Rankine cycle. No data for the extraction is reported in any of the two cases.

The operating pressures decrease with the maximum operating temperature of the thermal fluid in the literature results as well as in this work. In the high pressure turbine the literature reports values from 126 bar for molten salts to 100 in the case of Therminol VP1, while this work shows a larger decrease, from 125 bar to around 35 bar. In the medium pressure turbine the pressure decrease from the 11 bar when using molten salts, to 2.1–2.5 in all other five cases. The ones in the literature show values from 10 to 17 bar for the medium pressure (Montes et al., 2009a,b; Palenzuela et al., 2011), when reported. Similarly, the low-pressure turbine operates at 6.5 bar for the molten salts and only 1.1 bar for all six synthetic thermal fluids. This pressure is not reported in some cases presented in the literature. Finally, the exhaust pressures shown

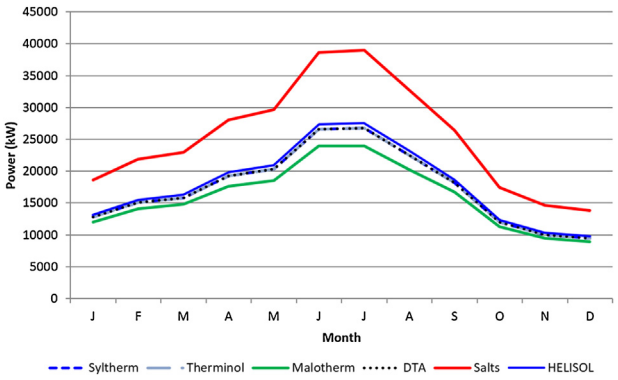

Fig. 2 – Profile of the power production over time for the six thermal fluids.

for the synthetic fluids are in the range of 0.08 bar for the optimization while Palenzuela et al. (2011) show values in the range of 0.18–0.31 bar and Halb et al. (2012) and Morin et al. (2010) present values from 0.06–0.2 bar.

Fig. 2 shows the profile of the production of electricity for the six thermal fluids operating 8760 h during the entire year. During summer, a peak of 40 MW can be reached using molten salts as HTF, while in November and December minimum values just below 20 MW can be achieved. For the synthetic fluids it is possible to see that the maximum production capacity is 30% lower compared to the use of molten salts. The power production profile follows the solar availability in all cases. On average, the facility using Malotherm fluid produces 16 MW while if salts are used as an HTF, the production capacity reaches 25 MW. In between we have the other four fluids, with an average production of around 18 MW.

4.2. *Effect of maximum fluid temperature on plant efficiency*

Once the performance of a CSP facility has been evaluated using different HTF's, the process model is used to study the effect of the maximum operating temperature of an HTF in the power production. For this evaluation, the turbine is assumed

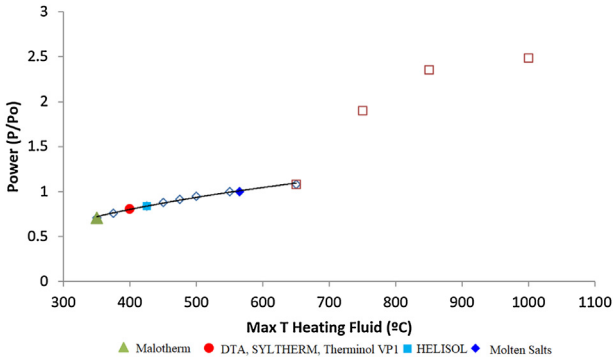

Fig. 3 – Effect of operating temperature of the fluid on the power production. Reference: Molten salts.

to operate at 100% load. Fig. 3 shows the decrease in the power produced relative to a reference that, for this case, is the facility that uses molten salts. A correlation, eq. (2), is developed for further evaluation of fluids and for fluid selection purposes as a function of their maximum operating temperature. It can be used as a simple rule of thumb to estimate the production of power in the context of prescreening promising HTF's.

$$\text{Power(MW)} = 0.6015 \cdot \text{Ln}(T_{max}(^{o}\text{C})) - 2.8031 \quad (2)$$

The efficiency of the cycle increases with the temperature of the hot source as expected. The correlation developed is interesting towards comparing biomass and solar as resources. Note that, for a particular location where the weather conditions do not jeopardize the cooling (cold end), the performance of the Rankine cycle only depends on the temperature of the hot source and therefore the results presented in Fig. 3 can allow estimating the yield of any other HTF. As a result, if the temperature further increases, the power extracted from the cycle will also increase, achieving the efficiencies that are found for a boiler as evaluated in a previous work (Guerras and Martín, 2020).

4.3. *Effect of the HTF on the consumption of water*

Water consumption can jeopardize the operation of solar facilities due to the limited availability in the regions of higher solar incidence. In previous work (Luceño and Martín, 2018) it was shown that even in arid regions, wet cooling towers were more sustainable than dry technologies. In addition, the consumption of water is another metric to evaluate the efficiency of the thermal cycle. Water consumption accounts for the losses due to evaporation (Ev), determined from the analysis of the operation of the plant, and blowdown (B), computed as eq. (3). The cycles of concentration (COC) are assumed to be 5 based on rules of thumb. It is assumed that the drift is negligible as it has been demonstrated for newly design facilities (Guerras and Martín, 2020).

$$B = \frac{Ev}{COC - 1} \quad (3)$$

The average consumption is 2.1 L/kWh, in the case of using molten salts. However, for the rest of the thermal fluids, the lower efficiency of the Rankine cycle results in larger water consumption ratios as a function of the highest operating temperature. HELISOL consumes around 3.0 L/kWh, DTA, Syltherm and Therminol VP1 consume an average of around 3.1 L/kWh while the Marlotherm reaches an average value of

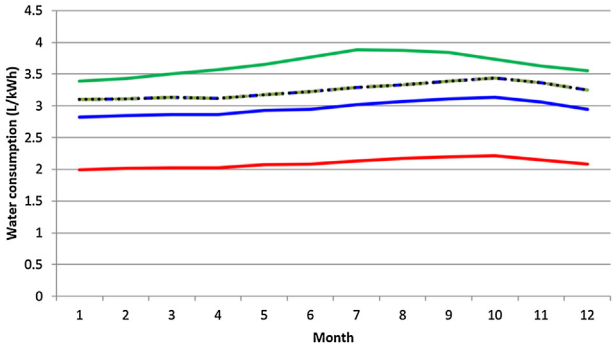

Fig. 4 – Water consumption over time.

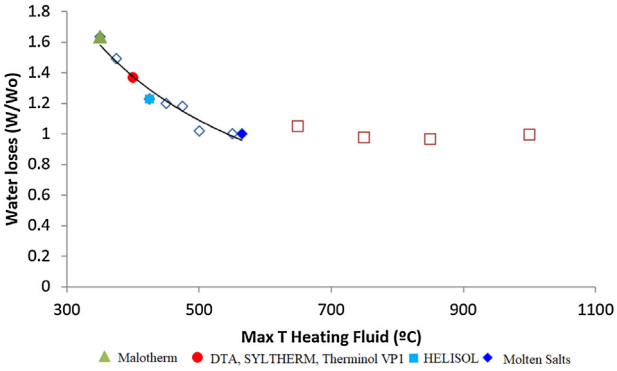

Fig. 5 – Effect of thermal fluid operating temperature on water consumption.

3.6 L/kWh. The monthly values are presented in Fig. 4. Typically, for CSP towers facilities values from 2.6 to 3.4 (Macknick et al., 2012) or 2.7 to 3.8 L/kWh (Stillwell et al., 2011) are reported. The range can be due to the use of different thermal fluids. The studies presenting values for VP1 report consumptions of water of 2.95 L/kWh (Palenzuela et al., 2013), similar to the ones obtained in this work, while molten salts-based facilities are reported to consume 2. 8 L/kWh (Stoddard et al., 2006). In addition. The location of the facility can also affect and modify the water consumption as presented in a previous paper (Guerras and Martín, 2020), where the water – energy nexus and the tower design is presented if synthetic thermal fluids are used. Rankine cycles in CSP plants operate at lower temperature at their hot end, increasing the cooling needs per kWh produced and the water consumption. However, if the temperature of the hot source of the cycle is above that of the molten salts, the relative water consumption reaches an asymptote, see Fig. 5.

Similarly as for the evaluation of the power production, assuming different maximum temperatures and full load operation at the turbine, the effect of the maximum operating temperature of the HTF on the water consumption is evaluated. It can be seen that the system is more efficient operating at higher temperatures. The consumption of water decreases with the maximum temperature of the HTF, see Fig. 5 and eq. (4). Beyond 565 °C an asymtote is reached

$$\text{Rel}(\text{Water}/\text{Water}_{Salts}) = 729 \cdot T_{max}(^{o}\text{C})^{-1.047} \quad (4)$$

Eq. (4) can be used to estimate the water consumption of Rankine cycles operating with other HTF's as a screening tool for novel synthetic fluids

4.4. *Economic evaluation*

In this section the major economic parameters of the processes using the six heat transfer fluids are discussed, including investment and production costs.

With regards to the investment cost, it is important to highlight that the turbine is sized for the power production under the design conditions presented in Table 5. In addition, the size of the units depends on the flows they process as well as on the fluid properties. In particular, the heat transfer coefficient determines the area of the heat exchangers involved. Fig. 6 shows the cost of different sections. The details of the units cost can be seen in the supplementary material. The distribution is similar in all the cases. One half of the cost comes from the solar field, the heat transfer units represent around 30%, while the turbine reaches 20% of the units costs. Table 5 shows the investment costs for the six different fluids. As a rule, the power production increases with the maximum operating temperature. However, the efficiency of the Rankine cycle results in the fact that the investment costs are larger for Marlotherm than for other fluids such as the rest of synthetic fluids, HELISOL, Syltherm, Therminol VP1 and Dowtherm A, and the molten salts. There is also an effect of the physical properties of the fluid on the flowrate of the thermal fluid as well as on the heat exchanger areas.

Table 4 also shows the production costs for electricity for the different heat transfer fluids. In the supplementary material the different items considered for the production costs are presented. The values are in the range from 0.12 €/kWh to 0.21 €/kWh. In general, the production cost of electricity decreases with the hottest temperature of the HTF. This is because of the higher yield and efficiency of the thermodynamic cycle. The effect of the properties of the fluid cannot be seen in the performance of the Rankine cycle but on the economics of the facility. For fluids with the same maximum operating temperature, Dowtherm A, Syltherm and Therminol VP1, the differences in the economics are related to the physical properties of the fluid, namely, the heat capacity, that determines the flow of liquid required to absorb the power from the sun, and the liquid film resistance, that determines the area of the heat exchangers. Corrosion issues are considered within the amortization of the units. As a result, HELISOL shows the lowest production cost among the synthetic oils, showing lower investment cost than any other HTF, but a production cost for the electricity 33% higher than using molten salts.

5. Conclusions

A techno economic analysis has been performed to evaluate the operation of solar thermal plants operating with six different heat transfer fluids, Malotherm, Therminol VP1, Dowtherm A, Syltherm, HELISOL and molten salts. A mathematical optimization framework has been developed to evaluate the operating and an economic analysis has been performed to estimate the investment and electricity production costs. The different physical properties of the fluids as well as their range of operating temperatures determine the power production, the consumption of water involved and the electricity costs.

On average over a year, using Malotherm as heat transfer fluid allows producing an average of 16 MW while if molten salts are used, up to 25 MW can be produced. The production capacity of the other fluids, DTA, Syltherm, HELISOL and Therminol VP1, reaches an average value of around 18 MW. However, the investment cost is not directly related to the power production, since the larger the production capacity the larger the turbine, that represents a large share in the investment cost. Furthermore, the area of the heat exchangers is directly related to the physical properties of the fluids resulting in the fact that, for the same maximum operating temperature, there is a 10% difference in the investment cost. The electricity production cost for the different HTF's ranges from 0.12 €/kWh to 0.21 €/kWh. This value is a direct result of the production capacity, taking into account the differences in the investment. Molten salts show the best performance, with the fifth largest investment, 400 M€, and the largest production capacity. The results presented do not only allow the comparison of the six HTF but also provide the information for the quick screening of novel HTF's using the correlations developed. Although the results are promising, a detailed engineering of the facility is required for a more accurate comparison.

Declaration of Competing Interest

The authors report no declarations of interest.

Acknowledgement

The authors would like to acknowledge PSEM3 research group for optimization software licenses.

Appendix A. Modeling details

Collector and heliostats field

The solar energy is redirected to a tower using heliostats where the heat thermal fluid is used. Typically, heliostats size ranges from 70 to 150 m^2. In our case we consider a mean value, 120 m^2. The tower has a heat exchanger in the top that is used to heat up the HTF by the concentrated solar energy.

The number of heliostats is computed for an average power of around 20 MW, taking Power in eq (A.1) equal to 25 MW (NREL 2010). The area needed in the heliostat field is calculated using the annual radiation as given by eq. (A.2).

$$A_{field} \cdot Rad_{annual} = Power \cdot t \tag{A.1}$$

$$A_{field} = n_h \cdot A_h \cdot \eta_h \tag{A.2}$$

Where the heliostat efficiency (η_h) is 90% and $Rad_{annual} = 520 kWh/m^2$

With that field of heliostats, for each month, we have the capability of gathering a certain amount of energy given by Eq (A.3). Note that, for the sake of simplicity in the presentation of the equations, from this point on we are not presenting the time period index in each one of them. The efficiency of a heliostat field depends on several parameters such as cosine losses (20%), shading and blocking (2% losses) (Moore et al., 2010), heliostat reflectivity (typical efficiency values range from 0.90 to 0.95 (Mancini, 2000) and transmission losses through the atmosphere (5% loses) (Ruiz Gernandez, 2009). To be on the safe side we consider a field efficiency (η_{field}) of 55%.

$$Energy = E_s = Rad_i \cdot t_d \cdot A_{field} \cdot \eta_{field} \tag{A.3}$$

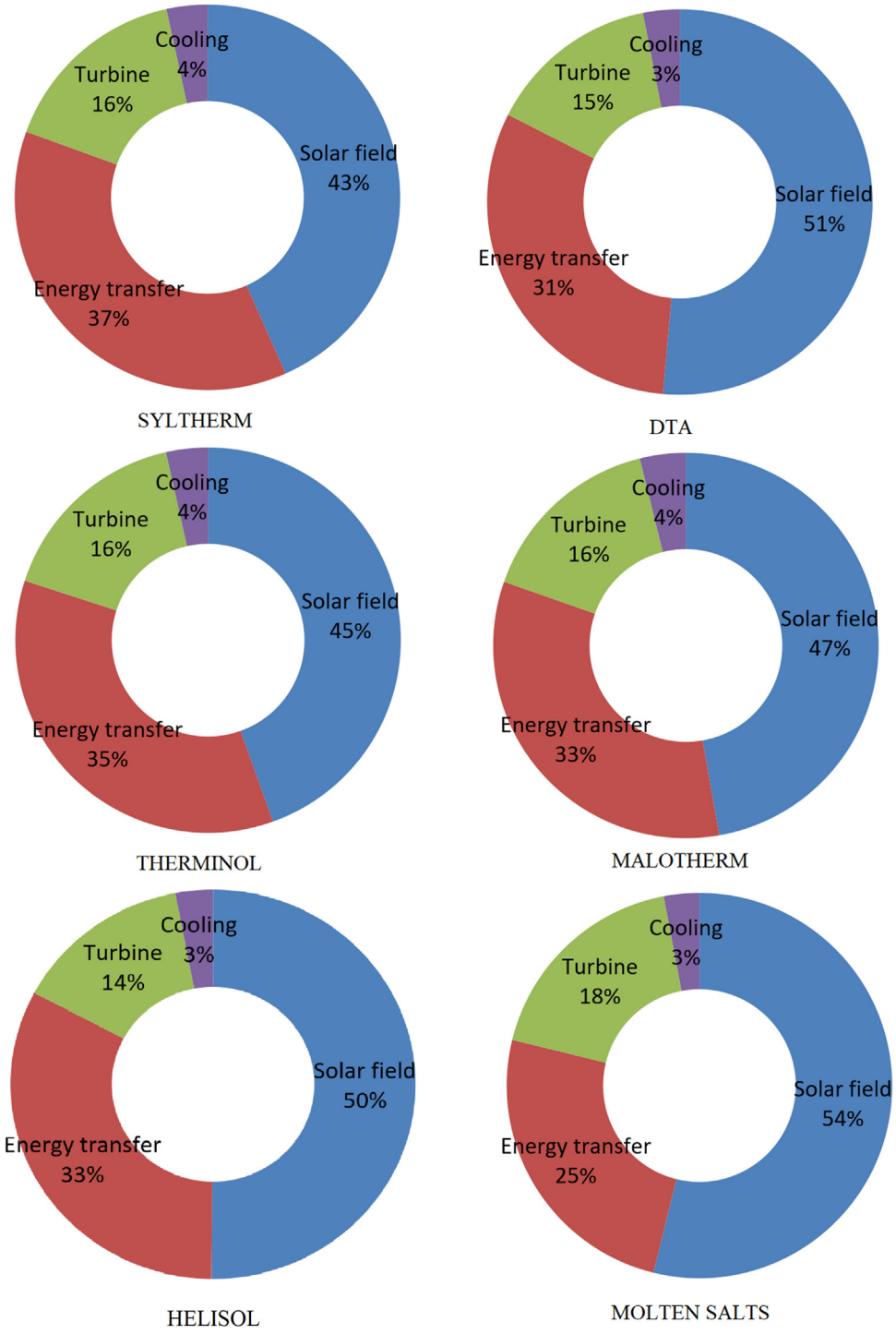

Fig. 6 – Distribution of unit costs for the different thermal fluids.

Table 4 – Main Units and costs for the various fluids.

Fluid	MaxP (MW)	Cooling (MW)	Investment Cost (M€)	Electricity Cost (€/kWh)
Heliosol	69	140	384	0.165
Dowtherm A	68	141	383	0.167
Syltherm	68	141	398	0.174
Therminol VP1	68	141	383	0.168
Malotherm	60	149	469	0.209
Salts	86	123	400	0.117

The heliostat field only collects energy during the sun hours. Eq. (A.4) determines que energy available for the collector:

$$\frac{Q_{(collector)}}{3600 \cdot h_s \cdot t_d} = E_s \quad \text{(A.4)}$$

The range of operating temperatures depends on the thermal fluid. DTA, Syltherm DOW 2019), and VP1 (Eastman, 2019) operate from 200 to 400 °C. Malotherm from 200 °C to 350 °C (SASOL 2019) and the molten salts from 290 °C and are heated

up to 565 °C using the energy collected from solar radiation. Thus, the flow of the HTF is calculated as eq. (A.5) during the sun hours with the heat capacity of the HTF (Dow 2019, Lie 2017; Eastman, 2019; Sasol 2019). The flow of the HTF in and out of the collector is the same, eq. (A.6):

$$Q_{(Colector)} = fc_{(HTF,Colector,Tank1)} \cdot \int_{T_{(Tank2,Colector)}}^{T_{(Colector,Tank1)}} cp_{HTF}\, dT \tag{A.5}$$

6 different synthetic fluids, heat transfer fluids (HTF), are considered. The heat capacities of the different fluids used are shown in Table A1.

$$fc_{(HTF,Tank2,Colector)} = fc_{(HTF,Colector,Tank1)}; \tag{A.6}$$

The flow rate of the HTF across the Power cycle cannot exceed the maximum possible flow produced at the collector corrected by the fraction of sun hours in a day, as presented in eq (A.7):

$$fc_{(HTF,Tank1,Spl1)} \leq \frac{(sun_{hours})}{24} \cdot fc^{(HTF,Tank2,Colector)}; \tag{A.7}$$

HTF operates in a closed cycle, modelled as in eq. (A.8):

$$fc_{(HTF,HX3,Tank2)} = fc_{(HTF,Tank1,Spl1)}; \tag{A.8}$$

Turbine system

A regenerative Rankine cycle is typically used (Moore et al., 2010). High pressure steam is generated using the HTF. The highest pressure at the turbine ranges typically from 30 to 125 bar (Pavlovic et al., 2012; Palenzuela et al., 2011, 2013; Xu et al., 2011; Bakos and Tsagas, 2002; Halb et al., 2012; Morin et al., 2010; Richter et al., 2011; Ghobeity et al., 2011). The steam is expanded into a mean pressure within the rage of 5 to 35 bar (Pavlovic et al., 2012; Palenzuela et al., 2013; Halb et al., 2012; Morin et al., 2010).

First, we present the mass and energy balances to the set of heat exchangers that transfer the solar energy stored in the HTF into the water/steam that follows the power cycle. In Fig. 3 we follow the HTF path. The flow of HTF from storage tank 1 is split so that part of HTF is used to heat up steam before being fed to the turbine, HX1, and the rest is used for a reheating stage, heat exchanger 4 (HX4), eq. (A.9)

$$fc_{(HTF,Tank1,Spl1)} = fc_{(HTF,Spl1,HX1)} + fc_{(HTF,Spl1,HX4)}; \tag{A.9}$$

The saturated steam at the operating pressure of the turbine is heated at HX1 employing the hot thermal fluids. The entalphy and entrophy of the different water stream, either as compressed liquid, saturated liquid, saturated vapor or superheated steam, were correlated as function of the pressure and temperature, eqs. (A.10–A.19) (Martín and Martín, 2013)

H and S for Compressed liquid

$$H\,(kJ/kg) = 4.2921 \cdot (T) + 4.1269 \tag{A.10}$$

$$S\left(\frac{kJ}{(kgK)}\right) = 1.1902 \cdot 10^{-5} \cdot (T)^3 - 3.7465 \cdot 10^{-3} \cdot (T)^2 + 4.5352 \cdot (T) + 0.64547 \tag{A.11}$$

H and S for Saturated liquid

$$H\,(kJ/kg) = 3.6082 \cdot 10^{-12}(T)^6 - 3.4120 \cdot 10^{-9}(T)^5 + 1.2303 \cdot 10^{-6}(T)^4 - 2.0306 \cdot 10^{-4}(T)^3 + 1.5552 \cdot 10^{-2}(T)^2 + 3.7216\,(T) + 3.0035 \tag{A.12}$$

$$S\left(\frac{kJ}{(kgK)}\right) = 1.0372 \cdot 10^{-12}(T)^5 - 8.6494 \cdot 10^{-10}(T)^4 + 2.8965 \cdot 10^{-7} \cdot (T)^3 - 5.6730 \cdot 10^{-5}(T)^2 + 1.6802 \cdot 10^{-2}\,(T) - 2.1997 \cdot 10^{-2} \tag{A.13}$$

H and S for Saturated Vapor

$$H\,(kJ/kg) = -6.5690 \cdot 10^{-12}(T)^6 + 6.3049 \cdot 10^{-9} \cdot (T)^5 - 2.3080 \cdot 10^{-6}(T)^4 + 3.8339 \cdot 10^{-4}(T)^3 - 3.0632 \cdot 10^{-2}(T)^2 + 2.7553\,(T) + 2.4957 * 10^3 \tag{A.14}$$

$$S\left(\frac{kJ}{(kgK)}\right) = -2.0373 \cdot 10^{-12}(T)^5 + 1.8589 \cdot 10^{-9}(T)^4 - 7.1901 \cdot 10^{-7}(T)^3 + 1.6112 \cdot 10^{-4}(T)^2 - 2.8904 \cdot 10^{-2}\,(T) + 9.1915 \tag{A.15}$$

H and S for Superheated steam (Up to 10 bar)

$$H\,(kJ/kg) = \left(-6.3293 \cdot 10^{-6} \cdot (P\,(bar)) + 3.3179 \cdot 10^{-4}\right) \cdot (T)^2 + (0.0124 \cdot (P\,(bar)) + 1.8039)\,T + (-6.0707\,(P\,(bar)) + 2504.6) \tag{A.16}$$

$$S\left(\frac{kJ}{(kgK)}\right) = 9.42 \cdot 10^{-10}(T)^3 - 3.09 \cdot 10^{-6}(T)^2 + 5.24 \cdot 10^{-3} \cdot (T) + \left(6.8171 \cdot (P(bar))^{(-0.069455)}\right) \tag{A.17}$$

H and S for Superheated steam (10 bar -150 bar)

$$H\,(kJ/kg) = \left(-1.1619 \cdot 10^{-13}(P\,(bar))^2 - 8.7596 \cdot 10^{-12}\,(P\,(bar)) - 2.2611 \cdot 10^{-10}\right)(T)^4 + \left(4.298 \cdot 10^{-10}(P\,(bar))^2 + 3.276 \cdot 10^{-8}\,(P\,(bar)) + 7.313 \cdot 10^{-7}\right)(T)^3 + \left(5.801 \cdot 10^{-7}(P\,(bar))^2 - 4.6 \cdot 10^{-5}\,(P\,(bar)) - 5.009 \cdot 10^{-4}\right)(T)^2 + \left(3.383 \cdot 10^{-4}(P\,(bar))^2 + 0.02947 \cdot (P\,(bar)) + 2.195\right)(T) + \left(-0.072042 \cdot (P\,(bar))^2 - 7.7877 \cdot (P\,(bar)) + 2440.8\right) \tag{A.18}$$

$$S\left(\frac{kJ}{(kgK)}\right) = \left(1.5719 \cdot 10^{-11}\,(P\,(bar)) + 7.4013 \cdot 10^{-10}\right) \cdot (T)^3 + \left(-1.0074 \cdot 10^{-10}(P\,(bar))^2 - 3.0171 \cdot 10^{-8}\,(P\,(bar)) - 2.8872 \cdot 10^{-6}\right)(T)^2 + \left(9.4914 \cdot 10^{-8}(P\,(bar))^2 + 2.9097 \cdot 10^{-5}\,(P\,(bar)) + 5.0938 \cdot 10^{-3}\right) \cdot (T) \left(4.1223 \cdot 10^{-5}(P\,(bar))^2 - 0.028841 \cdot (P\,(bar)) + 5.9537\right) \tag{A.19}$$

Table A1 – Heat capacities of the different HTF's.

HTF	C_p (kJ/kg K)	Reference	h(kW/m^2 K)	Reference
Molten Salts	Composition: 60%$_{w/w}$ $NaNO_3$ -40% $_{w/w}$ KNO_3 $C_p = 1.443 + 0.000172 \cdot T(^\circ C)$	Liu et al. (2017)	1.4	Wallas (1990)
DTA	$C_p = 1.493 + 0.00274 \cdot T(^\circ C)$	Dow (2019a)	0.8	Wallas (1990); DOW (2019a)
Syltherm	$C_p = 1.5742 + 0.0017076T(^\circ C)$	Dow (2019b)	0.45	Wallas (1990); DOW (2019b)
VP1	$C_p = 1.4864 + 0.0028229T(^\circ C)$	Eastman (2019)	0.8	Wallas, 1990; Eastman, 2019)
Malotherm	$C_p = 1.52 + 0.0031872T(^\circ C)$	(SASOL, 2019)	0.56	Wallas (1990); SASOL (2019)
HELISOL	$C_p = 1.609 + 0.00188T(^\circ C)$	Jung et al. (2015)	0.45	Wallas (1990); Jung et al. (2015)

Thus, the energy provided by the heat trasnfer fluid, calculated by eq. (A.20), corresponds to the energy transferred to the steam in HX1 as given by eq. (A.21):

$$Q_{(HX1)} = -fc_{(HTF,Spl1,HX1)} \int_{T_{(Spl1,HX1)}}^{T_{(HX1,Mix1)}} cp_{salt}\, dT \tag{A.20}$$

$$Q_{(HX1)} = fc_{(Wa,HX2,HX1)} \cdot \left(H_{steam,(HX1,Turbine1)} - H_{steam,(HX2,HX1)}\right) \tag{A.21}$$

Eq. (A.22) is used to make sure that the feed to HX1 is saturated:

$$P_{turb1} \cdot 760 = e\left(A(Wa) - \frac{B(Wa)}{\left(C(Wa) + T_{(HX2,HX1)}\right)}\right) \tag{A.22}$$

For each heat exchanger in the system we allow that a minimum approach temperature of 10 °C. The hot fluid leaving HX1 is mixed with the HTF from Tank 1. The mixing is modeled using eq. (A.23–A.26).

$$fc_{(HTF,HX1,Mix1)} = fc_{(HTF,Spl1,HX1)} \tag{A.23}$$

$$fc_{(HTF,HX1,Mix1)} + fc_{(HTF,HX4,Mix1)} = fc_{(HTF,Mix1,HX2)} \tag{A.24}$$

$$fc_{(HTF,Spl1,HX4)} = fc_{(HTF,HX4,Mix1)} \tag{A.25}$$

$$fc_{(HTF,HX1,Mix1)} \int_{T_{(HX1,Mix1)}}^{T_{(Mix1,HX2)}} cp_{HTF}\, dT + fc_{(HTF,HX4,Mix1)} \int_{T_{(HX4,Mix1)}}^{T_{(Mix1,HX2)}} cp_{HTF}\, dT = 0 \tag{A.26}$$

The flow of thermal fluid from Mix1 is used to evaporate the saturated water coming from HX3 in HX2. HX2 is modelled using eqs. (A.27–A.30)

$$Q_{(HX2)} = -fc_{(HTF,Mix1,HX2)} \cdot \int_{T_{(Mix1,HX2)}}^{T_{(HX2,HX3)}} cp_{HTF}\, dT = 0 \tag{A.27}$$

$$Q_{(HX2)} = fc_{(Wa,HX3,HX2)} \cdot \left(H_{steam,(HX2,HX1)} - H_{liq,(HX3,HX2)}\right) \tag{A.28}$$

$$fc_{(Wa,HX3,HX2)} = fc_{(Wa,HX2,HX1)} \tag{A.29}$$

$$fc_{(HTF,HX2,HX3)} = fc_{(HTF,HX3,Tank2)} \tag{A.30}$$

The HTF leaving HX2 are used in HX3 to heat up the compressed liquid stream already at P_{turb1} from HX6. HX3 is modelled using mass and energy balance given by Eqs. (A.31–A.34)

$$Q_{(HX3)} = -fc_{(HTF,HX2,HX3)} \int_{T_{(HX2,HX3)}}^{T_{(HX3,Tank2)}} cp_{HTF}\, dT \tag{A.31}$$

$$Q_{(HX3)} = fc_{(Wa,HX6,HX3)} \cdot \left(H_{liq,(HX3,HX2)} - H_{liq,(HX6,HX3)}\right) \tag{A.32}$$

$$fc_{(Wa,HX6,HX3)} = fc_{(Wa,HX3,HX2)} \tag{A.33}$$

$$fc_{(Wa,HX1,Turbine1)} = fc_{(Wa,HX2,HX1)} \tag{A.34}$$

The superheated steam is sent from HX1 to the high pressure turbine. We consider that high, medium and low pressure turbines are available. All of them are modelled similarly. Isentropic expansion is assumed in all turbines, with an efficiency, η_s, of 0.9 (Nezammahalleh et al., 2010). Therefore, the stream exiting the high pressure turbine can be calculated using eqs. (A.35–A.41)

$$\eta_{real} = \frac{H_{steam,(Turbine1,\ HX4)} - H_{steam,(HX1,\ Turbine1)}}{H_{steam,(isoentropy)} - H_{steam,(HX1,\ Turbine1)}} \tag{A.35}$$

Where

$$H_{steam,(isoentropy)} = f\left(p_{(Turbine1,HX4)}, T^*_{(Turbine1,HX4)}\right) \tag{A.36}$$

T^* corresponds to the isoentropic temperature after the expansion so that eq. (A.37) must hold.

$$s_{steam,(HX1,Turbine1)} = f\left(p_{(HX1,Turbine1)}, T_{(HX1,Turbine1)}\right) = f(p_{(Turbine2,HX4)}, T^*_{(Turbine1,HX4)}) \tag{A.37}$$

Eq. (A.38) is used to ensure that the steam exiting the turbine is superheated:

$$p_{turb2} \cdot 760 = e\left(A(Wa) - \frac{B(Wa)}{(C(Wa) + T_{turb1min})}\right) \tag{A.38}$$

$$T_{(Turbine1,HX4)} > T_{turb1min} \tag{A.39}$$

In addition, the efficiency of the turbien depends on the load correcting the isentropic efficiency. Correlations from the literature are used to compute those losses:

$\nu = (-1.0176 \cdot (Load)^4 + 2.4443 \cdot (Load)^3 - 2.1812 \cdot (Load)^2 + 1.0535 \cdot Load + 0.701)$ (Jüdes et al., 2009) (A.40a)

$\nu = 1 - \left(0.191 - 0.409 \cdot Load + 0.218 \cdot (Load)^2\right)$ (NREL, 2019) (A.40b)

$\nu = 0.4097 \cdot Load + 0.5903$ (Erhart et al., 2011) (A.40c)

Therefore, the actual efficiency is given by eq. (A.41):

$$\eta_{real} = \eta_s \nu \tag{A.41}$$

The power produced by expanding the steam at the high pressure turbine is given by eq. (A.42):

$$W_{(Turbine1)} = fc_{(Wa,HX1,Turbine1)} \cdot \left(H_{steam,(HX1,Turbine1)} - H_{steam(Turbine1,HX4)}\right) \tag{A.42}$$

The superheated steam is reheated up in HX4 using a fraction of the total flow of HTF stored in Tank1. Next, the stream is fed to the medium pressure turbine. HX4 is modeled using eqs. (A.43–A.44)

$$Q_{(HX4)} = fc_{(Wa,Turbine1,HX4)} \cdot \left(H_{steam,(HX4,Turbine2)} - H_{steam,(Turbine1,HX4)}\right); \tag{A.43}$$

$$Q_{(HX4)} = -fc_{(HTF,Spl1,HX4)} \cdot \int_{T_{(Spl1,HX4)}}^{T_{(HX4,Mix1)}} cp_{HTF} dT \tag{A.44}$$

In the medium pressure turbine, the steam is expanded to a lower pressure. A fraction of the stream is used in the regenerative section of the cycle, to HX6, while the rest is used in the low-pressure turbine where it is expanded exiting as saturated vapor within 0.05 bar to 0.31 bar (Pavlovic et al., 2012; Palenzuela et al., 2011; Halb et al., 2012; Morin et al., 2010; Ghobeity et al., 2011). The stream splitter located after the medium pressure turbine is modelled by eq. (A.45):

$$fc_{(Wa,HX4,Turbine2)} = fc_{(Wa,Turbine2,HX6)} + fc_{(Wa,Turbine2,Turbine3')}; \tag{A.45}$$

The exhaust steam is condensed in HX5, eq. (A.46). The liquid is reheated at HX6 using the extraction from the turbine

$$Q_{(HX5)} = fc_{(Wa,Turbine3,HX5)} \cdot \left(H_{liq,(HX5,HX6)} - H_{steam(turbine3,HX5)}\right); \tag{A.46}$$

The energy from HX5 is removed from the system using a cooling tower, see section 2.1.3. The stream exiting HX6 must be liquid. To save energy, a liquid stream is compressed up to P_{turb1}. To ensure that the stream exiting HX6 is liquid eq. (A.47) is used:

$$T_{(HX6,HX3)} \leq T_{turb2min}; \tag{A.47}$$

Where $T_{turb2min}$ is the temperature of saturation, computed using Antoine equation, at the operating pressure in HX6. The power generated at the high, medium and low pressure turbines given by eq. (A.48) is to be optimized.

$$W_{total} = W_{(Turbine1)} + W_{(Turbine2)} + W_{(Turbine3)}; \tag{A.48}$$

Cooling tower

A cooling tower is used to cool down the water used to condensate the exhaust steam from the third body of the turbine. The actual operation is a function of the atmospheric conditions, freshwater and air temperatures and humidity and represents a limit to the operation of the production facility. We use the Mickley method to evaluate the performance of the cooling tower (Geankoplis, 1993).

The equilibrium line for the air - water system at a given total pressure is computed as given by eq. (A.49), sequentially computing, for any given temperature, the vapor pressure, the saturating moisture, and the air enthalpy:

$$T_i \rightarrow P_{v,sat} \rightarrow Y_{i,sat} \rightarrow H_i\,(t_i, Y_i) \tag{A.49}$$

Next, the operating line is computed using eq. (50) given by an energy balance to the air and the water.

$$VdH = Ldh = Lc_L dt_L = Ldt_L \tag{A.50}$$

We use c_L =1 kcal/(kg°C) for simplicity in the form of the equations

$$\frac{H_2 - H_1}{t_{L2} - t_{L1}} = \frac{L}{V} \tag{A.51}$$

The liquid flow (L) is calculated assuming that the cooling water used in HX5 can only be heated up between 8 to 10 °C from the inlet temperature, that of the water in the environment, as given by eq. (A.52) since this increment in the temperature determines the water evaporative loses (Perry and Green, 1997)

$$8 \leq \left(T_{(HX5,Cooling)} - T_{(Cooling,Mix2)}\right) \leq 10 \tag{A.52}$$

We assume that the flow of air is within 1.3 to 1.5 times the minimum required by the operation (Geankoplis, 1993).

Rules of thumb (Perry and Green, 1997; Ahmetovic et al., 2010) are used to impose a lower bound of the water losses by evaporation, eq. (A.53):

$$fc_{(Wa,Cooling,Snk1)} \geq 1.8 \cdot 0.00085 \cdot fc_{(Wa,HX5,Cooling)} \left(T_{(HX5,Cooling)} - T_{(Cooling,Mix2)}\right) \tag{A.53}$$

The humid air temperature is computed discretizing an energy balance across the tower including the Lewis relationship, eq. (A.54–A.55)

$$h_i a S dZ\,(t_L - t_i) = Ldh = VdH = k_y a S dZ\,(H_i - H) \tag{A.54}$$

$$\frac{H_i - H}{t_i - t_L} = -\frac{h_L}{k_y} \tag{A.55}$$

Where the slope $(-h_L/k_y)$ is between -3 and -10 in industry and eqs. (A.56–A.57).

$$\frac{k_y\ a\ S\ dZ(H_i - H)}{k_y c_h\ a\ S\ dZ(t_i - t_g)} = \frac{VdH}{Vc_h dt_g} \tag{A.56}$$

$$\frac{(H_i - H)}{(t_i - t_g)} = \frac{dH}{dt_g} \tag{A.57}$$

See Martín and Martín (2013) for the details on the discretization. An upper bound for the air moisture of 95% is assumed.

Appendix B. Supplementary data

Supplementary material related to this article can be found, in the online version, at doi:https://doi.org/10.1016/j.cherd.2021.01.030.

References

Ahmetovic, E., Martín, M., Grossmann, I.E., 2010. Optimization of water consumption in process industry: Corn – based ethanol case study. Ind. Eng. Chem. Res. 49 (17), 7972–7982.

Almena, A., Martín, M., 2015. Techno-economic analysis of the production of epichlorohydrin from glycerol. Ind. Eng. Chem. Res. 55 (12), 3226–3238.

Junta de Andalucía. www.agenciaandaluzadelaenergia.es/Radiacion/radiacion1.php, 2012 (last accessed January 2013).

https://spanish.alibaba.com/g/therminol.html Last accessed December 2019.

Bakos, G.C., Tsagas, N.F., 2002. Technical feasibility and economic viability of a small-scale grid connected solar thermal installation for electrical-energy saving. Applied Energy 72, 621–630.

Barberena, J.G., Larrayoz, A.M., Sánchez, M., Bernardos, A., 2016. State of the art of heliostat field layout algorithms and their comparison. Energy Proc. 93, 31–38.

Collado, F.J., Guallar, J., 2019. Quick design of regular heliostat field for commercial solar tower power plants. Energy 178, 115–125.

Crespi, F., Toscani, A., Zani, P., Sánchez, D., Manzolini, G., 2018. Effect of passing clouds on the dynamic performance of a CSP tower receiver with molten salt heat storage. Appl. Energy. 229, 224–235.

de la Fuente, E., Martín, M., 2019. Optimal coupling of waste and concentrated solar for the constant production of electricity over a year. AIChE J. 65 (7), 1–11.

DOW, 2019a. Dowtherm a heat transfer fluid product technical data dow.

DOW, 2019b. Syltherm 800 heat transfer fluid product technical data dow.

Dowling, A.W., Zheng, T., Zavala, V.M., 2017. Economic assessment of concentrated solar power technologies: a Review. Renewable Sustainable Energy Revs 72, 1019–1032.

Eastman, 2019. Technical data sheet therminol® Vp-1 heat transfer fluid. Eastman.

Erhart, T., Eicker, U., Infield, D., 2011. Part-load characteristics of Organic-Rankine-Cycles. In: Proceedings of the 2nd European Conference on Polygeneration, Tarragona, Spain, 30 March–1 April 2011, pp. 1–11.

Fernández, A.G., Lasanta, M.I., Pérez, F.J., 2012. Molten salt corrosion of stainless steels and low-Cr steel in CSP plants. Oxi. Metals. 78 (5-6), 329–348.

Geankoplis, C.J., 1993. Transport Processes and Unit Operations, 3rd Edition. Prentice Hall Upper Saddle River, New Jersey. U.S.A.

Ghobeity, A., Noone, C.J., Papanicolas, C.N., Mitsos, A., 2011. Optimal time-invariant operation of a power and water cogeneration solar-thermal plant. Sol Energy 85, 2295–2320.

Guerras, L.S., Martín, M., 2020. Sustainable design of natural draft cooling towers for renewable based power plants. Appl Energy 263, 114620.

Halb, P., Blanco-Marigorta, A.M., Erlach, B., 2012. Exergoeconomic comparison of wet and dry cooling technologies for the Rankine cycle of a solar thermal power plant. Proceedings of ecos 2012 - the 25th international conference on efficiency, cost, optimization, simulation and environmental impact of energy systems 300-1, 300-314.

International Energy Agency, IEA, Paris 2010. Technology Roadmap Concentrating Solar Power France.

Janjai, S., Laksanaboonsong, J., Teesaard, T., 2011. Potential application of concentrating solar power systems for the generation of electricity in Thailand. Appl Energy 88, 4960–4967.

Jüdes, M., Vigerske, S., Tsatsaronis, G., 2009. Optimization of the Design and Partial-Load Operation of Power Plants Using Mixed-Integer Nonlinear Programming. In: Kallrath, J., Pardalos, P.M., Rebennack, S., Scheidt, M. (Eds.), Optimization in the Energy Industry. Energy Systems. Springer, Berlin, Heidelberg, pp. 193–220.

Jung, C., Dersch, J., Nietsch, A., Senholdt, M., 2015. Technological perspectives of silicone heat transfer fluids for concentrated solar power. Energy Proc. 69, 663–671.

Kuravi, S., Trahan, J., Yogi Goswami, D., Rahman, M.M., Stefanalos, E.K., 2013. Thermal energy storage technologies and systems for concentrating solar power plants. Progress in Energy and Comb. Sci 39, 285–319.

Leonardi, E., Pisani, L., Les, I., Mutuberria, A., Larrayoz, A., Rohani, S., Schottl, P., 2019. Techno. Economic heliostat field optimization: Comparative analysis of different layouts. Energy 180, 601–607.

Li, X., Wang, Z., Yang, M., Yuan, G., 2019. Modeling and simulation of a novel combined heat and power system with absorption heat pump based on solar thermal power plant. Energy 186, 115842.

Liu, T.L., Liu, W.R., Xu, X.H., 2017. Properties and heat transfer coefficients of four molten-salt high temperature heat transfer fluid candidates for concentrating solar power plants. IOP Conf. Series: Earth and Environ. Sci. 93 (2017), http://dx.doi.org/10.1088/1755-1315/93/1/012023, 012023.

Luceño, J.A., Martín, M., 2018. Two-step optimization procedure for the conceptual design of a-frame systems for solar power plants. Energy 165, 483–500.

Macknick, J., Newmark, R., Heath, G., Hallett, K.C., 2012. Operational water consumption and withdrawal factors for electricity generating technologies: a review of existing literature. Environ. Res. Lett. 7, 045802, http://dx.doi.org/10.1088/1748-9326/7/4/045802.

Mahmoudimehr, J., Sebhati, P., 2019. A novel multi-objective dynamic programming optimization method: performance management of a solar thermal power plant as a case study. Energy 168, 796–814.

Mancini, T.R., 2000. Catalog of Solar Heliostats. Tech. Rep. No. III - 1/00, IEA SolarPACES, Köln. Germany.

Martín, M., 2016. Industrial chemical process. In: Synthesis and Design. Elsevier, Oxford.

Martin, M., 2015. Optimal annual operation of the dry cooling system of a Concentrated Solar Energy Plant in the South of Spain. Energy 84, 774–782.

Martin, M., Martín, M., 2017. Cooling limitations in power plants: optimal multiperiod design of natural draft cooling towers. Energy 135, 625–636.

Martín, L., Martín, M., 2013. Optimal year-round operation of a concentrated solar energy plant in the south of Europe app. Thermal Eng. 59, 627–633.

Montes, M.J., Abánades, A., Martínez-Val, J.M., Valdés, M., 2009a. Solar multiple optimization for a solar-only thermal power plant, using oil as heat transfer fluid in the parabolic trough collectors. Sol Energy 83, 2165–2176.

Montes, M.J., Abánades, A., Martínez-Val, J.M., 2009b. Performance of a direct steam generation solar thermal power plant for electricity production as a function of the solar multiple. Sol Energy 83, 679–689.

Moore, R., Vernon, M., Ho, C.K., Siegel, N.P., Kolb, G.J., 2010. Design considerations for concentrating solar power tower systems employing molten salt. Sandia Report Sand2010-6978, Albuquerque, U.S.A.

Morin, G., Richter, P., Nitz, P., 2010. New method and software for multivariable technoeconomic design optimization of CSF plants (last accessed December 2012) www.mathcces.rwth-aachen.de/_media/5people/richter/pascalrichter-2010-solarpaces.pdf.

Mutuberria, A., Pascual, J., Guisado, M.V., Mayor, F., 2015. Comparison of heliostat field layout design methodologies and impact on power plant efficiency. Energy Proc. 69, 1360–1370.

Nezammahalleh, H., Farhadi, F., Tanhaemami, M., 2010. Conceptual design and techno-economic assessment of integrated solar combined cycle system with DSG technology. Sol Energy 84, 1696–1705.
Noone, C.J., Torrilhon, M., Mitsos, A., 2012. Heliostat field optimization: a new computationally efficient model and biomimetic layout. Solar. Energ. 86 (2), 792–803.
NREL, 2011. Concentrated solar power projects.
NREL, 2019. SAM. https://sam.nrel.gov/node/68897.
Palenzuela, P., Zaragoza, G., Alarcón-Padilla, D.C., Guillén, E., Ibarra, M., Blanco, J., 2011. Assessment of different configurations for combined parabolic-trough (PT) solar power and desalination plants in arid regions. Energy 36, 4950–4958.
Palenzuela, P., Zaragoza, G., Alarcón-Padilla, D.C., Blanco, J., 2013. Evaluation of cooling technologies of concentrated solar power plants and their combination with desalination in the Mediterranean area. Appl. Therm, Engng 50, 1514–1521.
Pavlovic, T.M., Radonjic, I.S., Milosavljevic, D.D., Pantic, L.S., 2012. A review of concentrating solar power plants in the world and their potential use in Serbia Renew. Sust. Energ. Revs. 16, 3891–3902.
Perry, R.H., Green, D.W., 1997. Perry's Chemical Engineer's Handbook. McGraw-Hill, New York, U.S.A.
Polimeni, S., Binotti, M., Moretti, L., Manzolini, G., 2018. Comparison of sodium and KCl-MgCl2 as heat transfer fluids in CSP solar tower with sCO2 power cycles. Sol Energy 162, 510–524.
Richter, P., Abraham, E., Morin, G., 2011. In: Dobnikar, A., Lotric, U., Ster, B. (Eds.), Optimisation of concentrating solar thermal power plants with neural networks. , pp. 190–199, Icannga 2011, part i, lncs 6593.
Ruiz Gernandez, Valeriano, 2009. La electricidad solar térmica, tan lejos, tan cerca. Fundación Naturgy.
SASOL, 2019. Marlotherm® heat transfer fluids. SASOL.
Sau, S., Corsaro, N., Crescenzi, T., D'Ottavi, C., Liberatore, R., Licoccia, S., Russo, V., Tarquini, P., Tizzoni, A.C., 2016. Techno-economic comparison between CSP plants presenting two different heat transfer fluids. Appl Energy 168, 96–109.
Schell, S., 2011. Design and evaluation of esolar's heliostat fields. Sol Energy 85 (4), 614–619.
Sinnot, R.K., 1999. Coulson and Richardson, Chemical Engineering, third ed. Butterworth Heinemann, Singapur.
Slocum, A.H., Codd, D.S., Buongiorno, J., Forsberg, C., McKrell, T., Nave, J.C., Papanicolas, C.N., Ghobeity, A., Noone, C.J., Passerini, S., Mitsos, A., 2011. Concentrated solar power on demand. Sol Energy. 85 (7), 1519–1529.
Sole, A., Falco, Q., Cabeza, L.F., Nevew, P., 2018. Geometry optimization of a heat storage system for concentrated solar power plants. Renew. Energy. 123, 227–235.
Stillwell, A.S., King, C.W., Webber, M.E., Duncan, I.J., Hardberger, A., 2011. The energy-water nexus in Texas. Ecol. Soc. 16 (1), 2 http://www.ecologyandsociety.org/vol16/iss1/art2/.
Stoddard, L., Abiecunas, J., O'Connell, R., NREL report. NREL/SR-550-39291 2006. Economic, Energy and Environmental benefits of concentrating solar power in California.
Tanimizu, K., Hooman, K., 2013. Natural draft dry cooling tower modelling. Heat Mass Trans. 49, 155–161.
Ustun, I., Karaku, C., Yagli, H., 2020. Empirical models for estimating the daily and monthly global solar radiation for Mediterranean and Central Anatolia region of Turkey Int. J. Global Warm 20 (3), 249–275.
Vidal, M., Martín, M., 2015. Optimal coupling of biomass and solar energy for the production of electricity and chemicals. Comp. Chem. Eng 72, 273–283.
Wallas, S.M., 1990. Chemical Process equipment. In: Selection and Design. Butterworth-Heinemann, Elsevier, Oxford UK.
Xu, C., Wang, Z., Li, X., Sun, F., 2011. Energy and exergy analysis of solar power tower plants Appl. Therm Engng. 31, 3904–3913.
Yagli, H., Karakus, C., Koc, Y., Cevik, M., Ugurlu, I., Koc, A., 2019. Designing and exergetic analysis of a solar power tower system for Iskenderun region Int. J. Exergy. 28 (1), 96–112.
Zhang, H.L., Baeyens, J., Degreve, J., Caceres, G., 2013. Concentrated solar power plants: review and design methodology. Renew. Sust. Energy Revs 22, 466–481.